Mon. Not. R. Astron. Soc. **000**, 000–000 (0000) Printed 1 February 2008 (MN LATEX style file v1.4)

# Interaction between the Intergalactic Medium and Galactic Outflows from Dwarf Galaxies

I. Murakami[1] and A. Babul[2]

[1] *National Institute for Fusion Science, Toki-shi, Gifu-ken 509-5292, Japan*

[2] *Department of Physics & Astronomy, University of Victoria, P. O. Box 3055, Victoria, BC V8W 3P6 Canada*

arXiv:astro-ph/9906084v1 4 Jun 1999

1 February 2008

## ABSTRACT

We have carried out 2D hydrodynamical simulations in order to study the interaction between supernova-powered gas outflows from low-mass galaxies and the local intergalactic medium (IGM). We are specifically interested in investigating whether a high pressure IGM, such as that in clusters of galaxies, can prevent the gas from escaping from the galaxy, as suggested by Babul and Rees (1992). We find that this is indeed the case as long as ram pressure effects are negligible. The interface between the outflow and ambient IGM is demarcated by a dense expanding shell formed by the gas swept-up by the outflow. A sufficiently high IGM pressure can bring the shell to a halt well before it escapes the galaxy. Galaxies in such high pressure environments are however, more likely than not, to be ploughing through the IGM at relatively high velocities. Hence, they will also be subject to ram pressure, which acts to strip the gas from the galaxy. We have carried out simulations that take into account the combined impact of ram pressure and thermal pressure. We find that ram pressure deforms the shell into a tail-like structure, fragments it into dense clouds and eventually drags the clouds away from the galaxy. The clouds are potential sites of star formation and if viewed during this transient phase, the galaxy will appear to have a low-surface brightness tail much like the galaxies with diffuse comet-like tail seen in z=1.15 cluster 3C324. The stars in the tail would, in time, stream away from the galaxy and become part of the intracluster environment.

In contrast, the relatively unhindered outflows in low density, low temper-

© 0000 RAS

ature environments can drive the shells of swept-up gas out to large distances from the galaxy. Such shells, if they intersect a quasar line-of-sight, would give rise to Ly $\alpha$ absorption lines of the kind seen in quasar spectra. In addition, the fact that outflows from low-mass galaxies can extend out to distances of 40 kpc or more indicates that such galaxies may have played an important role in polluting the intergalactic medium with metals.

**Key words:** galaxies:dwarf – inter galactic medium

## 1 INTRODUCTION

The study of dwarf galaxies has important implications for our current understanding of processes governing the formation of galaxies, stars, and large scale structure in general. The generally accepted models for structure formation via hierarchical clustering predict the existence of a large number of dwarf galaxies and that these galaxies are expected to be the sites of the earliest star formation (see White & Frenk 1991).

Although dwarf galaxies are the most numerous type of galaxies in the nearby universe, their numbers are far fewer than theoretical predictions (Ferguson & Binggeli 1994). Furthermore, the observations also seem to suggest that the smallest galaxies are among the youngest rather than the oldest, and this phenomena appears to be independent of environment. For example, many of the Local Group dwarf spheroidals and dwarf irregular galaxies appear to have formed a significant fraction of their stars in starbursts at $z \lesssim 1$ (see, for example, Van den Bergh 1994 and Tolstoy 1999). Deep imaging studies of intermediate redshift ($0.4 \lesssim z \lesssim 1.0$) clusters (e.g. Dressler et al. 1994; Couch et al. 1994, 1998) have found that most of the blue galaxies responsible for the Butcher-Oemler effect are small late-type spirals or irregular galaxies. It has been suggested that these galaxies are starburst dwarf galaxies (Koo et al. 1997) that eventually fade away or star-forming remnants of 'harrassed' small galaxies that will eventually evolve into the cluster dwarf spheroidal population (Moore et al. 1996; Moore, Lake, & Katz 1998). Similarly, detailed analyses of the faint blue galaxies that numerically dominate the field galaxy population at intermediate redshifts ($0.4 \lesssim z \lesssim 1.0$) indicates that a significant fraction of the very faint blue galaxies are small (and therefore, dwarf) galaxies that are actively forming stars at a relatively recent epoch (see Babul & Ferguson 1996 and references therein; Campos 1997; Driver & Fernandez-Soto 1998; Fioc & Rocca-Volmerange 1999).

The discrepancy between the theoretical expectation that small galaxies ought to be

among the oldest and the observational evidence to the contrary can either be due to the fact that hierarchical clustering model does not provide a complete description of structure formation particularly on the scales of interest, or that the astrophysics underlying the formation of dwarfs galaxies is not well understood, with the latter being the more accepted of the two possibilities. For example, it has long been recognized that dwarf galaxies are rather fragile systems that their formation and subsequent evolution, in fact their very character, is likely to be strongly affected by both internal and external conditions. The 'galaxy harrassment' model of Moore et al. (1996; 1998), the models advocating catastrophic mass loss following supernovae explosions (Larson 1974, Saito 1979, Vader 1986, Dekel & Silk 1986), and models that argue that star formation in these systems is strongly modulated by the internal and external UV radiation field (e.g. Babul & Rees 1992; Efstathiou 1992; Kepner, Babul & Spergel 1997; Norman & Spaans 1997; Spaans & Norman 1997; Corbelli, Galli & Palla 1997) are all based on the fragility of the dwarf systems.

The 'galaxy harrassment' mechanism of Moore et al. (1996; 1998) operates only in high density enviroments. Based on results of numerical simulations, Moore et al. have proposed that multiple, high-speed encounters between small disk galaxies and the large massive galaxies in the cluster enviroment can cause multiple starbursts in, as well as significant mass loss from, the lower mass galaxies. The interactions would rearrange the internal structure of the smaller galaxies, converting them into much more resilient, compact dwarf elliptical-like galaxies. Moore et al. also suggested that the continued harrassment of the debris tails — material torn from the original galaxies — will create tidal shocks that will promote further condensations and formation of dwarf galaxies. In this scenario, the most numerous class of galaxies in clusters have formed at moderate redshifts.

With regard to the impact of UV radiation on the star formation in dwarf galaxies, Babul & Rees (1992) and Efstathiou (1992) have discussed in detail how an ionizing flux of an intense metagalactic UV background, such as that established by quasars and early starbursts, can prevent the gas in halos with shallow potential wells from cooling and forming stars until $z \lesssim 1$, in spite of the fact that the halos themselves may have formed at some earlier epoch, by initially keeping the gas ionized and latter, by suppressing the formation of molecular hydrogen, the only coolant available to metal-poor gas (see Kepner, Babul & Spergel 1997). However, analytic calculations (Rees 1986; Ikeuchi 1986) and subsequent numerical studies (Katz, Weinberg & Hernquist 1996; Thoul & Weinberg 1996; Quinn, Katz, & Efstathiou 1996; Navarro & Steinmetz 1997; Forcada-Miro 1997) show that photoheating

most strongly affects halos with circular velocities $v_c \lesssim 30 - 35$km s$^{-1}$. Larger halos are largely unaffected. These limits, however, should be treated with some caution because none of these studies considered the impact of UV radiation from the very first stars on further star formation. In addition, all numerical studies except that of Kepner et al. (1997) ignored the fact that before metal-poor gas could cool and form stars, the ambient conditions must allow for the formation of neutral hydrogen, and even Kepner et al. (1997) only explored models involving spherical collapse. Subsequent studies by Corbelli, Galli & Palla (1997), Norman & Spaans (1997), and Spaans & Norman (1997) have gone much further. The latter authors, for example, considered halos with total masses spanning the range $10^8 - 10^{12} M_\odot$ and found that even if a halo does not get 'hung-up' by the background UV radition, the star formation in disk-like protogalaxies will initially proceed very slowly because the backreaction of star formation on the ionization and chemical equilibrium can greatly impact upon the abundance of $H_2$. The tight coupling between the radiation field and star formation rate is reduced only when the gas is sufficiently enriched. Consequently, the onset of massive starbursts, if any, even in Magellanic-type systems will be delayed until $z \sim 1$.

Once stars do form, there appears to a consensus, at least among the theorists, that the dwarf galaxies, due to their low escape velocities, will suffer supernova-driven outflows (eg. Larson 1974, Saito 1979, Vader 1986, Dekel & Silk 1986). Whether or not such outflows result in catastrophic loss of the interstellar medium is likely to depend on a variety of factors, such as the energy input in the interstellar medium (ISM), the ellipticity of the ISM distribution, etc. (see De Young & Heckman 1994). However, it is worth noting that the catastrophic loss of the gas for a galaxy and the subsequent quenching of the star formation provide a natural explanation for the low surface brightness and low metal abundances of dwarf galaxies (eg. Dekel & Silk 1986, De Young & Gallagher 1990). It also provides an explanation for the apparently rapid disappearance of the large numbers of small blue galaxies (low mass starbursting systems) that dominate the galaxy number counts at very faint magnitudes (see Babul & Rees 1992, Babul & Ferguson 1996).

Although supernova-driven outflow is an important aspect of any theoretical discussion of dwarf galaxy evolution, there has been, until recently, quite limited observational evidence for the existence of starburst-driven mass loss. The most detailed and convincing evidence was first reported by Meurer et al. (1992), who found a kpc-scale 'superbubble' of ionised gas expanding at $\sim$ 100 km/s in the core of the post-starburst dwarf galaxy NGC1705. This has now been followed up by Marlowe et al. (1995), who have studied a large sample

of starbursting dwarf amorphous galaxies and found evidence for outflows in approximately half of them. Also, Heckman et al. (1995) have argued that X-ray emission from dwarf galaxy NGC1569 is a signature of starburst-driven outflow.

Generally, it is assumed that if the starburst imparts sufficient energy to the affected fraction of the ISM to unbind it from the galaxy's gravitational potential well, then this material will be ejected from the galaxy. The situation is not as simple. The supernova rate needs to be high enough so that the remnants percolate the galaxy's interstellar medium in a time short compared to the remnant's radiative timescale (see, for example, Dekel & Silk 1986). In addition, Babul & Rees (1992) have noted that whether or not the outflow actually escapes from the low mass galaxy also depends on the state of the local intergalactic medium (IGM). The thermal pressure due to the IGM will resist the flow of material out of the galaxy. They argued that in regions of high pressure, such as in clusters of galaxies, the outflow would not be able to expand beyond the extent of the galaxy's dark halo and hence, will eventually accrete back onto the galaxy, allowing the galaxy to engage further star formation . In regions of low thermal pressure, the outflow would escape unhindered.

One consequence of the thermal-confinement picture is that there ought to be correlations between the properties of dwarf galaxies and their environment. For example, the low mass galaxies in high pressure environments, by virtue of being able to retain a greater fraction of their gas, ought to be more luminous and more metal-rich than comparable galaxies in the field. In clusters of galaxies, one would expect the dwarf galaxy population to exhibit a radial luminosity and metallicity gradients, with the galaxies closer to cluster center being, on the average, brighter and more metal-rich (Babul & Rees 1992). Recent observations seem to suggest that such trends do exist. For example, Secker (1996) finds significant color gradient in the radial distribution of dE galaxies in Coma, with redder galaxies tending to be closer to the cluster center. Secker interprets the color gradient as indicative of a metallicity gradient. Similar radial color gradients have also been detected in other clusters (O. Lopez-Cruz, private communications). Secker, Harris & Plummer (1997) also find that redder dE galaxies are also more luminous. More generally, dwarf elliptical galaxies are found only in high-density environments such as clusters of galaxies or clustered around giant galaxies (Vader & Sandage 1991; Ferguson 1992; Vader & Chaboyer 1993). According to the the thermal confinement scenario, this is because low mass galaxies in high density environments are more luminous and have higher surface brightness, and are therefore easier to detect. Ferguson & Sandage (1991) and Vader & Sandage (1991) have argued that the number ratio

of early-type dwarfs to early-type giant galaxies is correlated with cluster richness with the ratio being larger for richer clusters. The bright nucleated dE galaxies have only been sighted in clusters and even in this environment, they tend to be much more centrally concentrated than the non-nucleated dEs (Ferguson & Binggeli, 1994). We also be note that if the intrinsic mass function of the galaxies is steeply rising towards the low mass end, as predicted by most hierarchical galaxy formation theories, then this steep end ought to be easiest to observe in high density envrionments since the galaxies of a given mass in such environments will tend to be relatively brighter. Luminosity functions of cluster galaxies with steep rise at the low luminosity end have been observed by, for example, Trentham (1988).

In this first of a series of studies, we investigate the idea of pressure-confined outflows put forth by Babul & Rees (1992). Specifically, we use a 2D hydrodynamical code to study the influence of the local IGM on outflows from spherically symmetric dwarf galaxies, such as the Local Group dwarf spheroidals and cluster dwarf ellipticals, in various different environments. Admittedly, spherically symmetric dwarf galaxies are likely to lose the greatest amount of ISM; however, in the present study, we are not so much concerned with the degree of mass loss as with the interaction of the outflow with the local intergalactic environment. In addition, dwarf galaxies are not static objects. In high-density cluster environments, for example, the dwarfs are likely to be ploughing through the local IGM at relatively high velocities. In such cases, they will also be subject to ram pressure and contrary to the action of thermal pressure, ram pressure acts to strip the ISM from the galaxy (Gunn & Gott 1972; Gisler 1976; Lea & De Young 1976; Toyama & Ikeuchi 1980; Fabian, Schwarz, & Forman 1980; Takeda, Nulsen, & Fabian 1984; Gaetz, Salpeter, & Shaviv 1987; Portnoy, Pistinner & Shaviv 1993; Balsara, Livio, & O'Dea 1994). We also investigate the combined impact of ram pressure and thermal pressure under different conditions. In §2, we define our model for the dwarf galaxy and outline the methods used in this investigation. In §3.1, we discuss the evolution of outflows subject only to thermal pressure and in §3.2, we consider the combined impact of thermal and ram pressure. In §4, we discuss the possible observational consequences of the interaction between the outflows from dwarf galaxies and the surrounding intergalactic medium. Finally, we summarize the our findings in §5.

## 2 MODEL

Since we are interested in low-mass galaxies, we will adopt as a fiducial galaxy, a system whose dark halo mass is $M = 10^9 M_\odot$ and the circular velocity characterizing the gravitational potential of the system is $V_{\rm c} \approx 18$ km/s. For simplicity, we assume that the virialized dark halos have spherically symmetric density profiles

$$\rho(r) \propto 1/(r^2 + r_{\rm c}^2), \tag{1}$$

where $r_{\rm c}$ is the core radius set by the numerical resolution of our simulation, which is either 0.1, 0.2, or 0.25 kpc. The corresponding one-dimensional velocity dispersion of the galaxy is $\sigma \approx 25$ km/s. This velocity dispersion is somewhat larger than that of a typical Local Group dwarf spheroidal ($\sigma \sim 10$ km/s); on the other hand, the general characteristics of our system (i.e. low mass and shallow potential well) are comparable to those of the dwarf ellipticals (Peterson and Caldwell 1993) found in clusters of galaxies.

We assume a mass of $M_{gas} = 6 \times 10^7 M_\odot$ for the gas in the halo. In order to be susceptible to star formation, the gas must be at least marginally self-gravitating (eg. Mathews 1972). To satisfy this constraint, we require all the gas to be concentrated within a central 1 kpc of the halo and identify the centrally condensed baryonic system in the halo as the galaxy. All stellar activity, from star formation to supernova explosions, takes place in the galaxy.

The 'natural' rate for star formation in a self-gravitating gas cloud is

$$\dot{M}_* \propto \frac{M_g(t)}{t_{ff}}, \tag{2}$$

where $M_g(t)$ is the instantaneous mass of gas cloud and $t_{ff}$ is the free-fall timescale for the cloud (e.g. Dekel & Silk 1986). For the system under consideration, the star formation rate is $\sim 1\ M_\odot {\rm yr}^{-1}$. This rate is almost three orders of magnitude larger than that the maximum rate adopted by MacLow & Ferrara (1998) in their study. It is, however, comparable to the star formation rate in the faint blue galaxies as established from their redshifts and B magnitudes (Babul & Rees 1992). Furthermore, since the star formation is distributed over a region one kiloparsec in radius, the star formation rate per unit area of $\sim 1\ M_\odot {\rm yr}^{-1}{\rm kpc}^{-2}$ is comparable to that seen in typical starburst galaxies (Lehnert & Heckman 1996).

Soon after the onset of starburst, the massive stars will go supernova. If each supernova releases $10^{51}$ ergs, the rate of total energy released by the supernova explosions into the interstellar matter is

$$\dot{E}_{\rm SN} = 10^{49} \varepsilon_{\rm SN} \dot{M}_* {\rm ergs\ yr}^{-1}, \tag{3}$$

where $\varepsilon_{\rm SN}$ is the number of supernovae per $100 M_\odot$ of stars formed, and $\dot{M}_*$ is the star formation rate in units of $M_\odot {\rm yr}^{-1}$. In the solar neighbourhood, one has roughly one supernova for every 150 $M_\odot$ of baryons that form stars; hence, $\varepsilon_{\rm SN} \approx 0.67$. If starbursts make only high mass stars (see, for example, Rieke et al. 1993), then $\varepsilon_{\rm SN}$ would be larger. For present purposes, we assume that $\varepsilon_{\rm SN}\dot{M}_* = 1.4$.

Most of the energy released by the supernova will radiated away and only a small fraction, $\eta \approx 0.1$, will go towards heating the ISM (see Larson 1974; Dekel & Silk 1986; Babul & Rees 1992). The total rate of energy input to gas is then $\dot{E}_{\rm Heat} = \eta \dot{E}_{\rm SN} \approx 1.4 \times 10^{48}$ergs yr$^{-1}$. We assume that this energy input lasts for $2 \times 10^7$yr. The lifetimes of supernova Type II progenitors range from few$\times 10^6$– few$\times 10^7$ years, and we assume that the very first generation of SN explosions will disrupt the interstellar medium and quench further star formation.

As we will show in the following section, the energy input described above is sufficient to generate an outflows from the dwarf galaxy. This is neither surprising nor the thrust of the present work. Many previous works (eg. Larson 1974; Dekel & Silk 1986; Babul & Rees 1992) have already made this point. Here, we are more interested in studying how different local intergalactic conditions affect the outflow and the eventual fate of the expelled gas. Specifically, we focus on the influence of the thermal and ram pressures engendered by the intergalactic medium.

At the start of the simulation, the IGM gas is uniformly distributed across the entire simulation volume except in the galaxy, the central 1 kpc region of the halo. This distribution is not in equilibrium with the gravitational potential of the halo and in the absence of outflows from the galaxy, would accrete into the halo. In our simulations, this accretion is not important. The associated timescale is comparable to the total duration of a single simulation run and is much longer than all the dynamical timescale established by the outflows.

To study the influence of thermal component of the intergalactic pressure, we vary the value of $\widetilde{P}_{\rm IGM} \equiv nT$ from $10^{-2}$ to $10^5$ K cm$^{-3}$. The lower limit corresponds to an IGM of $n \sim 10^{-6}$ cm$^{-3}$ heated to the temperature of $T \sim 10^4$ K by photoionisation and the upper limit corresponds to pressures thought to exist in central regions of galaxy clusters. As we have already noted, observations indicate that starburst dwarf galaxies are found in all type of environments, especially at intermediate redshifts.

To study the effects of ram pressure, we allow the galaxy halo to have velocity, with respect to the IGM, ranging from $V = 400$ to 1000 km s$^{-1}$. The parameters for the cases discussed in this paper are summarized in Table 1.

We study the outflow and its interaction with the IGM using an axisymmetric Euler code (Norman & Winkler 1985; Yoshioka & Ikeuchi 1990; Murakami & Ikeuchi 1994). Following Norman & Winkler (1985), we include artificial viscosity in our simulations in order to treat shocks. We use the code to solve (in cylindrical coordinates)
the continuity equation:

$$\frac{\partial \rho}{\partial t} + \nabla \cdot (\rho \boldsymbol{v}) = 0, \tag{4}$$

the Euler equation:

$$\rho \left[ \frac{\partial \boldsymbol{v}}{\partial t} + (\boldsymbol{v} \cdot \nabla)\boldsymbol{v} \right] = -\nabla P - \rho \nabla \Phi, \tag{5}$$

the Poisson equation:

$$\nabla^2 \Phi = 4\pi G \rho_d, \tag{6}$$

and the energy equation:

$$\frac{\partial}{\partial t}(\rho \epsilon) + \nabla \cdot (\rho \epsilon \boldsymbol{v}) = -P \nabla \cdot \boldsymbol{v} + \mathcal{H} - \mathcal{L}. \tag{7}$$

In the above equations, $\epsilon$ is the specific internal energy, $\mathcal{H}$ and $\mathcal{L}$ are the heating and cooling rates respectively, and $\rho_d$ is the density of dark halo matter. We ignore the self-gravity of the baryonic system. We also ignore the depletion of gas as it forms stars as well as mass input from stellar winds and supernova explosions. The rest of the symbols have their usual meanings.

The heating rate, $\mathcal{H}$, is zero everywhere except in the galaxy itself, where for a brief time, the supernova explosions inject thermal energy into the ISM at a rate $\mathcal{H} = 3\dot{E}_{\rm Heat}/4\pi r_{\rm o}^3$, where $r_{\rm o} = 1$kpc. For the cooling rate, we consider two possibilities: A cooling rate for gas with primordial abundance (hereafter, referred to as 'primordial cooling') and a cooling rate for gas with cosmic abundance ($Z = 0.017$) determined by Allen (1973) (hereafter, referred to as 'metal cooling'). In order to compute the primordial cooling rate, we take into account radiative recombination, collisional ionisation, thermal bremsstrahlung, line emission and dielectric recombination (see Umemura & Ikeuchi 1987) for the gas of $n_H/n_{He} = 9$. For the metal cooling rate, we use a broken power-law fit of the results of Raymond, Cox & Smith (1976) who adopted the cosmic abundances (that is, $X = 0.73$, $Y = 0.25$, and $Z = 0.017$) tabulated by Allen (1973). In computing the heating rate due to supernova explosions, we

have already taken into account the fact that most of the energy will be lost via cooling radiation. To keep the cooling functions on during this time would mean that we would be double counting the cooling losses. Therefore, the cooling function is switched on after the supernova explosions cease.

## 3 RESULTS

We now discuss the results of our simulations. First, we shall consider cases where the outflows from dwarf systems are impeded only by the thermal pressure of the IGM. Subsequently, we shall consider cases where the dwarf system is acted upon by thermal as well as ram pressure.

### 3.1 The Impact of Thermal Pressure on the Outflow

Energy input from supernova explosions causes the interstellar medium in the galaxy to heat up to $T \sim 10^6$ K. As a consequence of the resulting pressure differential between the gas in the bubble and the IGM, the bubble expands and an outflow is established. At its maximum, the leading edge of the outflow has a velocity of order 200km s$^{-1}$. The outflow/expansion represents the conversion of some of the SN-injected thermal energy into kinetic energy. As in all outflow-type situations (e.g. see Castor, McCray & Weaver 1975 and references therein), the interaction between the outflow and the intergalactic medium leads to the formation of a dense shell consisting of the swept-up ISM and IGM. In Figures 1 – 4, we show the evolution of the outflow for models -2M, 0M, 3M and 4M (see Table 1). The results for gas subject to primordial cooling are qualitatively similar.

In cases where the IGM temperature is $T = 10^4$ K (models -2M and 0M/P), the leading edge of the outflow is supersonic and the interface between the outflow and the unperturbed IGM is demarcated by a shock. In models where the IGM temperature is $T = 10^7$ K, the outflow is always subsonic and, as expected, the gas ahead of the forming shell is also perturbed. In Figure 5, we show the radial pressure, density, temperature, and velocity profiles for models 0P and 0M. The left and right panels show the profiles for models 0P and 0M respectively during the expansion phase. In Figures 6 and 7, we show the expanding (left-hand panels) and contracting (right-hand panels) for models 4M and 4P, respectively. During the heating phase, the pressure in the bubble exceeds the IGM pressure and the heated gas begins to expand outward. At the head of the outflow, the swept-up ISM and

IGM begins to form a shell. Once the outflow is established and the heating stops, the gas in the cavity cools as a result of radiative as well as adiabatic cooling. The higher density gas closer to the center of the gas cools much more rapidly than lower density cavity gas behind the shell as a result of efficient radiative cooling. Eventually, all of the gas in the cavity cools.

Once the pressure in the cavity drops below that of the external IGM, the shell begins to decelerate. (The sweeping up of the IGM also decelerates the shell but in all but the low pressure cases, $[\widetilde{P}_{\rm IGM} \lesssim 10^2]$, the effect is not important.) With continued expansion, the pressure in the cavity may fall below that in the shell and a contact discontinuity forms at the boundary between the two. Once the shell velocity becomes comparable to the sound speed in the external IGM, the shell velocity stagnates. If a contact discontinuity has formed between the cavity gas and the inner boundary of the shell, then in the shell frame of reference, the inner shell boundary begins to expand inward into the cavity, led by a shock front which halts and thermalizes the outflowing cavity gas and also smoothes out the sharp pressure gradient. This inward expansion of the inner shell boundary has also been noted by Ciardi & Ferrara (1997).

In high pressure environments, the stagnation radius and the halting radius are, for all practical purposes, equivalent as the stagnation point is reached just before the shell is stopped. The inward expansion of the inner shell boundary is, however, evident in the right panels (collapsing phase) of Figures 6 and 7. In low pressure environments, the shell decelerates very slowly and there can be a large lag between the time when the shell velocity stagnates and when it comes to a halt. During this time, the outer shell continues to expand outward while the inner boundary begins to expand inward, and the shell thickness grows. For $\widetilde{P}_{\rm IGM} = 10^0$ (Figure 5), the stagnation occurs at $R \approx 20$ kpc.

As expected, the main difference between the metal and primordial cooling cases is the increased efficiency of radiative cooling in the former case. This is obvious both from the rapid evolution of the temperature profiles, the thinness of the shell and the dramatic drop in the temperature of the gas remaining in the galaxy. In fact once the heating stops, a small cooling flow is established as the gas flows back towards the potential minimum.

The maximum radius to which the shell expands depends on the IGM pressure. If the IGM pressure is low ($\widetilde{P}_{\rm IGM} \lesssim 10^2$), the shell can be driven well beyond the virial radius of the halo and into the intergalactic space. If, on the other hand, the IGM pressure is as high as in the central regions of clusters, the shell expands by a very small amount

before being halted. From a physical point of view, the evolution of the bubble-shell system is schematically similar to that of 'superbubbles' as sketched out by MacLow, McCray & Norman (1989) although, it should be noted that are differences between the configuration that they studied and those considered here. One consequence of this is that the bubble-shell expansion in our simulations is not self-similar.

The simulation results do, however, suggest that the radius of maximum expansion is related to the value of the IGM pressure as:

$$R_{\rm max} \approx 8.2 \left(\frac{\widetilde{P}_{\rm IGM}}{10^3}\right)^{-0.36} \quad {\rm kpc}, \tag{8}$$

with $R_{\rm max}$ for the metal cooling cases tending to be slightly smaller than that for the corresponding primordial cooling cases. In addition, preliminary numerical experiments indicate that $R_{\rm max}$ also depends, albeit weakly in the case of shallow potential wells of the kind under consideration in this paper, on the depth of the gravitational potential well of the halo in the sense that $R_{\rm max}$ decreases as $V_c$ increases.

During the expansion phase, the amount of intergalactic mass that is swept-up by the shell-bubble system is:

$$M_{\rm shell} \approx 6.3 \times 10^6 \left(\frac{n_{\rm IGM}}{10^{-4}{\rm cm}^{-3}}\right) \left(\frac{R}{10{\rm kpc}}\right)^3 \quad {\rm M}_\odot. \tag{9}$$

In all but cases 0P/M and -2M, the external pressure brings the shell-bubble system to a halt well before the swept-up mass exceeds the mass originally in the SN-heated bubble.

For models -2M, the shell continues expanding during the entire course of the simulation, expanding to distances greater than 40 kpc. In this case, the shell-bubble system would need to expand out to 98 kpc before the swept-up mass exceeds the initial mass. We can safely assume that the system will indeed expand out to this radius since $R_{\rm max}$ for this configuration is estimated to be $\sim 500$ kpc. However, we do not follow the expansion out to such radii.

For model 0P/M, the bubble-shell system expands beyond 21 kpc, the radius at which the swept-up mass equals that initial mass in the bubble. Thereafter, the leading front of the shell continues to evolve much like an 'Oort snowplow'. $R = 21$ kpc is also roughly the stagnation radius and therefore, while the outer shell radius continues to expand, the inner boundary expands inwards as described previously, sweeping through the cavity in $\sim 7 \times 10^8$ years. This inward propagating shock is stable against Rayleigh-Taylor instabilities because both the density gradient and pressure gradient have the same sign. And in this regard, the

inward moving shock is very different from the shell collapse that occurs in high pressure environments and that we discuss below.

Once the shell is brought to a halt, both gravity and the IGM pressure begin to force the system to contract. The timescale for the shell to fall back onto the central galaxy, assuming that all the gas has piled up in the shell and that the shell remains intact during the collapse, can be estimated as

$$\tau_{\rm crush} \sim \sqrt{\frac{M_{\rm bubble}}{4\pi R_{\rm max} P_{\rm IGM}}} \approx 5 \times 10^7 \left(\frac{\widetilde{P}_{\rm IGM}}{10^3}\right)^{-0.32} \ {\rm yrs}, \tag{10}$$

where we have used equation (8). This estimate matches the actual collapse time within a factor of 2. In computing $\tau_{\rm crush}$, we have assumed that in comparison to the pressure force, the gravitational force can be neglected; the pressure force exceeds the gravitational force by two orders of magnitude or more.

The bottom two panels of Figures 3 and 4 show the collapse of the shell in cases 3M and 4M, while the right panels in Figures 6 and 7 show the the radial pressure, density, temperature, and velocity profiles for models 4M and 4P, respectively, at different times during the collapse phase. The evolution of the SN-heated gas bubble as well as the shell during the collapse phase depends sensitively on the efficiency of cooling. In the metal cooling case, the cooling timescale of the gas in the bubble is generally shorter than the dynamical timescale and gas/shell collapses in a 'simple' fashion. In the primordial cooling case, however, the cooling timescale is larger than the dynamical timescale. As the gas/shell collapses, the gas is heated and the resulting increase in the pressure causes the shell to bounce. (See curves for $t = 6.1 \times 10^7$yr and $6.8 \times 10^7$yr in the right-hand panels of Figure 7.) The same, though a bit more pronounced, occurs in simulations with no radiative cooling.

Once the shell starts to collapse, it begins to buckle and deform into tentacle-like structures. This deformation is due to initially small perturbations that are present in the shell being enhanced by Raleigh-Taylor (R-T) instability. As discussed by Chevalier (1976) and others, a pressure-driven flow is R-T unstable if the pressure gradient (source of acceleration) and the density gradient have opposite signs. In numerical simulations of supernova explosions (e.g. Nagasawa, Nakamura, & Miyama 1988; Arnett, Fryxell, & Muller 1991; Hachisu et al. 1991), R-T instability manifests as well-defined mushroom-like features. This shape is a consequence of the fact that the structures develop outward. In present case, the shell is contracting. The features associated with the R-T instability are also mushroom-like;

however, the heads of the mushrooms develop inward where there is less volume and hence, merge with each other, giving rise to tentacle-like structures.

Whether R-T instability materializes in a numerical simulation and the extent to which it does depends sensitively on the resolution of the numerical simulation (Arnet et al. 1991). In Figure 8, we show the evolution of shell-bubble for model 3M during the collapse phase. The two left panels show the results corresponding to resolution $\mathrm{d}r = 0.2$ kpc and the two right panels show the results for exactly the same simulation but with $\mathrm{d}r = 0.1$ kpc.

In both cases, the shell buckles and tentacle-like features arise as it is forced to contract. In the higher resolution case, however, there are many more tentacle-like features, the shell itself is thinner and has a greater tendency to fragment forming small clouds. This is especially true of the lagging sections of shell. The presence of clouds and extended tentacles ensures that the collapse is not uniform. The lag between when the first parts of the shell reach the central region of the galaxy and when the clouds fall in is $\sim 1.3 \times 10^7$ yr. Once the shell has fragmented and the pressure surrounding the clouds has equilibrated, the clouds are only subject to gravitational forces.

### 3.2 The Impact of Thermal and Ram Pressure on the Outflow

As we mentioned in the introduction, galaxies in high-thermal-pressure environments such as clusters of galaxies are also moving, often supersonically, through the intracluster medium. The intracluster medium flowing through a galaxy results in the gas in the galaxy being subjected to ram pressure forces (in addition to the thermal pressure forces). The impact of the ram pressure is to strip away the gas in a galaxy, eventually denuding the galaxy of its gas content. Ram pressure stripping is thought to be the dominant mechanism by which galaxies in cluster environment lose their gas (Gunn & Gott 1972; Gisler 1976; Lea & De Young 1976) and consequently, a great deal of effort has gone into trying to understand the process, especially through the use of two-dimensional hydrodynamic simulations (eg. Takeda et al. 1984; Gaetz et al. 1987; Portnoy et al. 1993; Balsara et al. 1994 ).

In the case of galaxies moving through the intracluster medium at velocities comparable to or larger than the velocity dispersions of typical clusters ($v \sim 1000$km s$^{-1}$), the ram pressure forces can equal or exceed the thermal pressure forces (we shall continue to denote thermal pressure as $P_{\rm IGM}$):

$$\frac{P_{\rm ram}}{P_{\rm IGM}} \sim \frac{\rho v^2}{nkT} \sim \left(\frac{V_{\rm flow}}{\sigma_{dis}}\right)^2, \tag{11}$$

where $\sigma_{dis}$ is the velocity dispersions of clusters. Ram pressure effects can have significant impact on the outflow from the galaxies. At the very least, the expanding gas shell will not be spherically symmetric in spite of the fact that the outflow is. Upstream, the expanding shell is subject to both thermal and ram pressure ($P_{\rm IGM} + P_{\rm ram}$) while on the downstream side, the shell is largely unaffected by ram pressure. Consequently, the shell should therefore be oval-shaped. The halting distance of the shell should also reflect this asymmetry. For example, the upstream stopping distance of the shell associated with a galaxy moving at 1000 km/s through a $\widetilde{P}_{\rm IGM} = 10^3$ ICM should be comparable to the maximum expansion radius of the shell associated with a galaxy embedded in $\widetilde{P}_{\rm IGM} = 10^4$ ICM (see equation 8).

The snapshots in Figure 9 show the effect of ram pressure on the outflow from a dwarf galaxy described in the example above. The galaxy is moving at a velocity of $V_{\rm flow} =$ 1000km s$^{-1}$ through a medium characterized by $\widetilde{P}_{\rm IGM} = 10^3$ (Model 3MW). For reasons mentioned above, the expanding shell has an oval shape (Figure 9a). Once the upstream expansion of the shell is halted, ram pressure begins to drag the material in the shell downstream, distorting the shell (Figure 9b). The downstream side shell is also distorted by the eddying flow towards the center of potential well. The shell buckles and begins to fragment into high density clouds (Figure 9c,d). In time, the upstream segment of the shell is pushed back into the galaxy while the remains of the rest of the shell is distorted into a hyperboloid-like surface. The galaxy-shell system resembles a comet, with the main galaxy forming the head and the shell material being the tail. The dense clouds are cold and are potential sites of star formation. If this was to occur, one would expect the resulting galaxy to have a relative high surface brightness 'head' attached to a diffuse tail.

While the evolution of the outflow/shell in models 4PW/4MW are qualitatively similar to that in models 3PW/3MW (described above), this is not the case when the ambient thermal pressure is as high as $\widetilde{P}_{\rm IGM} = 10^5$ (models 5MW/5PW). In such circumstances, the combined pressure (ram + thermal) greatly exceeds the thermal pressure of the supernova heated gas. Even during the heating phase, heated gas is unable to expand upstream. Instead, the shell that forms at the interface between the supernova-heated gas and ambient intergalactic medium is quickly swept downstream and the galaxy loses most its gas in $\sim 2 \times 10^7$ years (Figure 10). Perpendicular to the flow, the heated gas manages to expand slight but the resulting larger cross-section presented to the oncoming wind only hastens the sweeping away of the gas.

Thus far, we have been considering the impact of ram pressure on a dwarf galaxy that

is moving at a velocity comparable to what one would expect of a galaxy in a rich cluster. We have also considered cases where the galaxy is moving at somewhat lower velocities, velocities comparable to what one would expect in poor clusters and galaxy groups.

Specifically, we consider cases where $\widetilde{P}_{\rm IGM} = \{10^2,\ 10^3\}$ and $V_{\rm flow} = \{400,\ 600\}$km s$^{-1}$, respectively. In these simulations, the thermal pressure is not overwhelmed by ram pressure and during the expansion phase, the results are similar to that in the no-wind case except that the shape of the expanding shell is not quite spherical. The main effect of the wind is to gradually drag downstream the more slowly collapsing tentacles and clumps. Most of the expelled gas manages to collapse back into the central regions but it too is eventually dragged out of the halo and carried downstream.

The clouds that form during the crushing and the fragmentation of the shell tend to have densities $n_H \geq 0.1{\rm cm}^{-3}$ and sizes $R_{\rm cl} \sim 0.1$–$0.5$ kpc. The cloud masses range between $M_{\rm cl} \approx 10^5$–$10^6 M_\odot$. Once formed, the clouds are accelerated by the wind. For a cloud at rest, the timescale for cloud to be accelerated to the escape velocity of the dwarf galaxy halo by ram pressure is

$$\begin{aligned} \tau &\sim \frac{v_{\rm esc} M_{\rm cl}}{P_{\rm ram} \pi R_{\rm cl}^2} \\ &= 2.6 \times 10^7 v_{\rm esc,20} M_{\rm cl,5} V_{\rm flow,3}^{-2} n_{\rm IGM,-4}^{-1} R_{\rm cl,-1}^{-2} {\rm yr}, \end{aligned} \tag{12}$$

where $v_{\rm esc,20} = v_{\rm esc}/20$ km s$^{-1}$, $M_{\rm cl,5} = M_{\rm cl}/10^5$ M$_\odot$, $V_{\rm flow,3} = V_{\rm flow}/10^3$ km s$^{-1}$, $n_{\rm IGM,-4} = n_{\rm IGM}/10^{-4}{\rm cm}^{-3}$, and $R_{\rm cl,-1} = R_{\rm cl}/0.1$ kpc. The clouds remain in the vicinity of the galaxy (i.e. within the dark halo of the galaxy) for approximately $10^8$ years before they are dragged away. The clouds are also subject to thermal evaporation, which will enhance the stripping rate (Nulsen1982).

## 4 DISCUSSION AND SPECULATIONS

One of the most important results that we draw from our work is that in cluster environments, the confinement of the supernovae-heated outflows from dwarf galaxies is complicated by the effects of ram pressure. If the ram pressure acting on a dwarf galaxy is much less than the thermal pressure of the local intergalactic medium, then, as described by Babul & Rees (1992), the outflow from the galaxy is indeed halted by the thermal pressure and the confined gas subsequently falls back onto the galaxy, providing fuel for a possible second burst of star formation. Otherwise, ram pressure alters the confinement picture in a very

significant fashion. Only a small fraction of the expelled gas manages to collapse back onto the central galaxy; most of it is swept away. If this is the case, it is difficult to understand how trends reported, for example, by Secker (1996) would arise unless there exist two different populations of dE galaxies, an original population that is centrally concentrated within the cluster and whose members have lower velocities, and a more extended, higher velocity population comprising of galaxies that fell into the cluster at some latter time. The outflows from the former group would be subject to thermal confinement and one would expect such galaxies to be brighter and redder on the average, much like the population of nucleated dEs. The more extended 'infall' population of dE galaxies, on the other hand, are likely to recover a very small fraction of the outflowing gas: If the outflow occurs while the galaxies are outside the cluster, thermal ICM pressure there is too low to effect any confinement. If the outflow occurs after the galaxies fall into the cluster, the ram pressure acting on the galaxies would sweep away the bulk of the gas.

In cases where the ram pressure is important, the gas that is swept away tends to be concentrated in small clouds — fragments of the shell that formed at the interface between the ICM and the outflowing material. Ordinarily, transfer of heat from the IGM and into the clouds via conduction would cause the clouds to evaporate. The magnetic fields that permeate cluster environments are likely to suppress thermal conduction and therefore, the clouds will maintain their integrity. The clouds are dense enough to support small episodes of star formation and because of their velocities and spatial distribution, we would expect that if the galaxy was observed while the clouds were forming stars, it would resemble a comet, with the actual galaxy forming the head and the distributed star forming regions tracing out the 'comet tail'. There are quite a few galaxies with 'comet-like' morphologies in $z = 1.15$ cluster 3C324 (Dickinson, private communications; Dickinson 1996). Drawing upon the results of our simulations, we speculate that these objects are galaxies whose interstellar medium is being stripped away and that some of the stripped material is undergoing star formation, giving rise to the diffuse tail-like structures. This would suggest the structures should have blue colors, possibly bluer than the colors of the central galaxy although it is difficult to quantify the expected difference in color between the 'head' and the diffuse 'tail' because infalling material collapsing onto the central galaxy may also cause the central galaxy to experience a burst of star formation.

Furthermore, we would argue that the tail-like structures are transient features that will eventually disappear. As noted above, the ram pressure accelerates the clouds to relatively

high velocities and, although once formed the stars are immune to effects of ram pressure, they will eventually disperse because of the velocity imparted at the time formation (in effect, the cloud velocity at the time). In cluster environments, where in fact stripping is most likely to occur, the high velocity stars would give rise to a diffuse population of intraclusters stars. Such a population of stars have recently been detected in Fornax (Theuns & Warren 1997) and Virgo (Ferguson, Tanvir & Von Hippel 1998).

As already noted, the evolution of the gas streaming out of dwarf galaxies in environments where the ICM pressure is low, is very different from that of dwarfs in hot, high density regions. The outflow triggered by the first generations of supernova explosions will give rise to a mass shell that, for all practical purposes, expands away from the galaxy and carries away its gas supply. The field dwarf galaxies, therefore, are likely to experience only one short episode of star formation.

The dense expanding shells and dense clumps will give rise to Ly $\alpha$ absorption lines in quasar spectra if lines of sight to the quasars intersect such structures. Here we consider the profiles of such absorption lines and the HI column densities associated with the absorption. As seen in the simulations, almost all of the galactic gas, $M_{gas}$, and the swept-up IGM are in the expanding shell. When the shell radius, $R_{\rm s}$, is much larger than 1kpc, the shell mass is

$$\begin{aligned} M_{\rm s} &\simeq M_{gas} + 4\pi\mu m_H n_{\rm IGM} R_{\rm s}^3/3, \\ &\simeq M_{gas}(1 + 0.06 R_{\rm s,30}^3 n_{\rm IGM,-6} M_{g,7.8}^{-1}), \end{aligned} \tag{13}$$

where $m_H$ is the mass of the hydrogen atom, $R_{\rm s,30} = R_{\rm s}/30$ kpc, $M_{g,7.8} = M_{gas}/6\times10^7 M_\odot$, and $n_{\rm IGM,-6} = 10^{-6}{\rm cm}^{-3}$. For simplicity, we assume that the gas has primordial abundance ($n_H/n_{He} = 9$) and therefore, $\mu = 1.3$. The swept-up gas mass dominates the shell mass once the shell expands beyond $R_{\rm s} \sim 77(M_{g,7.8}/n_{IGM,-6})^{1/3}$kpc. If the IGM density is higher, the swept-up mass can come to dominate sooner. For $n_{\rm IGM} = 10^{-4}{\rm cm}^{-3}$, the IGM density in outer regions of the clusters or the mean IGM density of the universe at $z = 3.5$, the swept-up mass becomes comparable to the galactic gas when $R_{\rm s} \sim 17 M_{g,7.8}^{1/3}$ kpc. The average hydrogen density of the shell is then

$$\begin{aligned} n_H &= 0.9 M_{\rm s}/(4\pi\mu m_H R_{\rm s}^2 \Delta R_{\rm s}){\rm cm}^{-3}, \\ &\simeq 1.5\times10^{-4} M_{g,7.8} R_{\rm s,30}^{-2} \Delta R_{\rm s,1}^{-1} \\ &\qquad \times(1 + 0.06 R_{\rm s,30}^3 n_{\rm IGM,-6} M_{g,7.8}^{-1}){\rm cm}^{-3}, \end{aligned} \tag{14}$$

where $\Delta R_{\rm s}$ is the width of the shell, and $\Delta R_{\rm s,1} = \Delta R_{\rm s}/1{\rm kpc}$.

If the gas is photoionised by a metagalactic UV flux and is in ionisation equilibrium, the number density of neutral hydrogen is given by $n_{\rm HI} \simeq n_H^2 \alpha_H / G_H J$, where $\alpha_H$ is the hydrogen recombination rate, and $G_H J_0$ is the photo-ionisation rate (see, for example, Black 1981). If $J_0$ is the UV flux at Ly limit ($J_0 = J_{21} \times 10^{-21}$ erg s$^{-1}$cm$^{-2}$Hz$^{-1}$sr$^{-1}$) and the spectrum of the background UV radiation is $J_\nu \propto \nu^{-1}$, then the neutral hydrogen number density is

$$\begin{aligned} n_{\rm HI} &\simeq 3.1 \times 10^{-9} T_4^{-3/4} J_{21}^{-1} M_{g,7.8}^2 R_{\rm s,30}^{-4} \Delta R_{\rm s,1}^{-2} \\ &\quad \times (1 + 0.06 R_{\rm s,30}^3 n_{\rm IGM,-6} M_{g,7.8}^{-1})^2 {\rm cm}^{-3}, \end{aligned} \tag{15}$$

where $T_4 = T/10^4$ K is the gas temperature. The HI column density at zero impact parameter through the shell is

$$\begin{aligned} N_{\rm HI} &\simeq 2 n_{\rm HI} \Delta R_{\rm s} \\ &\simeq 1.9 \times 10^{13} T_4^{-3/4} J_{21}^{-1} M_{g,7.8}^2 R_{\rm s,30}^{-4} \Delta R_{\rm s,1}^{-1} \\ &\quad \times (1 + 0.06 R_{\rm s,30}^3 n_{\rm IGM,-6} M_{g,7.8}^{-1})^2 {\rm cm}^{-2}. \end{aligned} \tag{16}$$

The column density depends on the shell radius. When the IGM density is low, $N_{\rm HI}$ decreases rapidly with increasing shell radius. However, once the swept-up mass becomes comparable to the galactic mass, the above equation suggests that $N_{\rm HI}$ becomes proportional to $R_{\rm s}^2$ but as we have seen in Figure 5, the shell thickness does not remain constant. At large radii, the shell thickness too increases as mass is swept-up and this increase in the shell width slows the growth of the HI column density.

Figure 11 shows the HI column density along a line-of-sight that has impact parameter, $p$, as a function of time for model -2M. The radius of the expanding shell is indicated by the upper horizontal axis. The radius is defined as the outermost boundary of the shell. For the background UV radiation, we use $J_{21} = 1.0$ and neglect any self-shielding of the UV flux. The HI column density through the center grows with time because of the cooling inflow of gas. On the other hand, the maximum value of the HI column density for lines with $p > 1$kpc decreases as the shell radius grows.

The shell motion and structure affects the shape of the absorption line. A typical line-of-sight intersects a shell in two places and therefore, one would expect to see two absorption lines separated in velocity space by $2V_{\rm s}\sqrt{R_{\rm s}^2 - p^2}/R_{\rm s}$ because of the expansion of the shell. When the separation between the two lines is small, thermal broadening of the lines can, however, cause the lines to overlap and blur, giving the impression of one broad line. Alterna-

tively, the combination of the two lines can give rise to double-horn features. The absorption profiles that take into account the velocity field and thermal broadening can be calculated according to Wang (1995).

Figures 12 and 13 show the absorption line profiles for model -2M at $t = 1.9 \times 10^8$yr (Figure 12) and for model 0M at $t = 2.9 \times 10^8$yr (Figure 13). The impact parameters are the same as in Figure 11. The double-horn line profiles caused by the two absorption line features are readily observed, particularly at low impact parameters. As the impact parameter is increased and the component of the expansion velocity along the line-of-sight becomes smaller, the separation between the two lines decreases and the overall width of the absorption feature become narrower. The double-horn feature in our plots are similar to those described by Wang (1995) except that Wang assumed a steady state outflow with lower gas density and relatively higher gas temperature resulting in shallower absorption lines.

The results for model 0M and -2M can be taken as examples of what we would expect if galactic winds were responsible for Ly $\alpha$ clouds at $z = 3 - 4$ and at $z < 1$, respectively. Recent KECK observations of Ly $\alpha$ forests by Lu et al.(1998) show us interesting absorption lines which have double horn profile: two absorption systems at $z_a = 2.95614$ in the spectrum of QSO1107+4847 and at $z_a = 3.62361$ in the spectrum of QSO1422+2309. These profiles are very much like one shown in Figure 13. They are associated with CIV absorption lines and located in the visinity of quasars within 3000km s$^{-1}$. If there are nearby galaxies in a cluster around the quasars, the profiles can be explained as consequence of metal-enriched galactic outflows.

Ciardi & Ferrara (1997) have proposed that a hot secondary halo that forms when the inner boundary of the shell re-expands back into the cavity would also produce Ly $\alpha$ absorption lines. The beginnings of this inward re-expansion is seen in our simulation of model 0M. The outer radius expanded out to the radius at which we stopped all our simulations well before the secondary halo had been established. We were, therefore, not able to explore its effects on quasar spectra.

Finally, the fact that outflow from low-mass galaxies can extend out to distances of 40 kpc or more indicates that such galaxies may have played an important role in polluting the intergalactic medium with metals at high redshifts. This possibility was first discussed by Silk, Wyse & Shields (1987). The ubiquity of the carbon features observed in quasar absorption systems at $z \approx 3$ (Cowie et al. 1995; Tytler et al. 1995; Songaila & Cowie 1996)

implies that metals were dispersed over a large region, if not uniformly, fairly early in the history of the Universe. The fact that the generally accepted hierarchical clustering models for structure formation suggest that at high redshifts, the Universe was dominated by halos with shallow potential wells and, as we have shown, the fact that the winds from these wells can spread out over large distances supports the scenario where early generations of dwarf galaxies are responsible for polluting the intergalactic medium.

## 5 SUMMARY

In this paper, we have sought to study the interaction between supernova-powered gas outflows from low-mass galaxies and the local intergalactic medium (IGM). We find that even if the supernova explosions are, in principle, able to expel the gas from a low-mass galaxy, they may not be able to do so if the thermal pressure of the local intergalactic medium is sufficiently high. The thermal pressure of the IGM resists the outflow, eventually bringing it to a halt. The confinement radius, the radius to which the gas can expand before being brought to a halt, depends on the IGM pressure as $R_{\rm max} \propto P_{\rm IGM}^{-0.36}$. The higher the IGM pressure, the smaller the confinement radius. We find that the thermal pressure of the hot intracluster medium in clusters of galaxies, for example, is large enough to prevent the gas from expanding much beyond the galaxy.

The interface between the outflow and quiescent IGM is demarcated by a dense expanding shell formed by the gas swept-up by the outflow. Once halted, the IGM pressure pushes the shell back into the galaxy. The collapsing shell is susceptible to Rayleigh-Taylor instability resulting in non-uniform collapse of the gas. The instability enhances small perturbations in the shell, causes it to deform into tentacle-like structures and eventually fragments into small clouds.

In high density, high temperature regions, the dwarf galaxies are also likely to be moving at high velocities and therefore, subject to the effects of ram pressure. When ram pressure is comparable or higher than the ambient thermal pressure, it can distort and fragment the shell into high density clouds that are then dragged away from the galaxy and carried downstream. These high density clouds are potential sites of star formation and the spatial distribution of stars newly born in these clouds will trace out a diffuse tail-like structure. We speculate that comet-like galaxies with diffuse tail seen in z=1.15 cluster 3C324 are such galaxies. The structure exhibited by these galaxies is temporary; it will dissolve away as

the stars stream away and become part of a diffuse population of stars in the intracluster environment.

In contrast, the relatively unhindered outflows in low density, low temperature environments can drive the shells of swept-up gas out to distances of 40 kpc or more from the galaxy. Such shells, if they intersect a quasar line-of-sight, would give rise to Ly $\alpha$ absorption lines of the kind seen in quasar spectra. Assuming that the Universe is permeated by a metagalactic UV flux, the absorption features correspond to HI column densities typically of order $10^{15}$ cm$^{-3}$. At small impact parameters, the velocity field of the expanding shell gives rise to double-horned absorption profiles. This feature weakens and disappears as the impact parameter increases. Finally, the fact that outflow from low-mass galaxies can extend out to distances of 40 kpc or more indicates that such galaxies may have played an important role in polluting the intergalactic medium with metals at early epochs.

## ACKNOWLEDGMENTS

This research was partially carried out at the Canadian Institute for Theoretical Astrophysics. We would like to thank to M. Dickinson for his helpful comments and discussions. We also thank the anonymous referee for helpful comments and poignant suggestions. I.M. acknowledges NSERC for a fellowship and A.B. acknowledges support from NSERC through an operating grant.

## REFERENCES

Allen C. W., 1973, in *Astrophysical Quantities*, 3rd edition. Athlone Press, London.

Arnett D., Fryxell B., Muller E., 1991, in *Supernovae*, Ed: S. E. Woosley, Springer, New York, p. 232

Babul A., Ferguson H. C., 1996, ApJ, 458, 100

Babul A., Rees M. J., 1992, MNRAS, 255, 346

Balsara D. S., Livio M., O'Dea C. P., 1994, ApJ, 437, 83

Black J. H., 1981, MNRAS, 197, 553

Castor J., McCray R., Weaver R., 1975, ApJ, 200, L103

Campos A., 1997, ApJ, 488, 606

Chevalier R. A., 1976, ApJ, 207, 872

Ciardi B., Ferrara A., 1997, ApJ, 483, L5

Corbelli E., Galli D., Palla F., 1997 ApJ, 487, L53

Couch W. J., Ellis R. S., Sharples R. M., Smail I., 1994, ApJ, 430, 121

Couch W. J., Barger A., Smail I., Ellis R. S., Sharples R. M., 1998, ApJ, 497, 188

Cowie L.L., Songaila A., Kim T.-S., & Hu E.M., 1995, AJ, 109, 1522

De Young D. S., Gallagher J. S. III, 1990, ApJ, 356, L15

De Young D. S., Heckman T., 1994, ApJ, 431, 598

Dekel A., Silk J., 1986, ApJ, 303, 39

Dickinson M., 1996, in *HST and the High Redshift Universe*, Eds: N. Tanvir, A. Aragon-Salamanca, J.V. Wall, World Scientific, London. (astro-ph/9612178)

Dressler A., Oemler A., Butcher H. R., Gunn J. E., 1994, ApJ, 430, 107

Driver S. P., Fernandez-Soto A., 1998, in *Dwarf Galaxies and Cosmology*, Eds: Thuan et. al. Editions Frontiers. (astro-ph/9805100).

Efstathiou, G., 1992, MNRAS, 256, 43P

Fabian A. C., Schwarz J., Forman W., 1980, MNRAS, 192, 135

Ferguson H. C., 1992, MNRAS, 255, 389

Ferguson H. C., Binggeli B., 1994, A&AR, 6, 67

Ferguson H. C., Sandage A., 1991, AJ, 101, 765

Ferguson H. C., Tanvir N. R., Von Hippel T., 1998, Nature, 391, 461 (astro-ph/9801228).

Fioc M., Rocca-Volmerange B., 1999, astro-ph/9902020

Forcada-Miró M. I., 1997, astro-ph/9712205

Gaetz T. J., Salpeter E. E., Shaviv G., 1987 ApJ, 316, 530

Gisler G. R., 1976, A&A, 51, 137

Gunn J. E., Gott J. R., 1972, ApJ, 176, 1

Hachisu I., Matsuda T., Nomoto K., Shigeyama T., 1991, ApJ, 368, L27

Heckman T.M., Dahlem M., Lehnert M.D., Fabbiano G., Gilmore D., Waller W. H., 1995, ApJ, 448, 98

Ikeuchi S., 1986, Astrophys. Space Sci., 118, 509

Katz N., Weinberg D. H., Hernquist L., 1996, ApJS, 105, 19

Kepner J., Babul A., Spergel D., 1997, ApJ, 487, 61

Koo D. C., Guzman R., Gallego J., Wirth G. D., 1997, ApJ, 478, 49

Larson R. B., 1974, MNRAS, 166, 585

Larson R. B., 1987, in *Starbursts and Galaxy Evolution*, Eds: T. Thuan, T. Montmerle, J. Tranthanhvan, Edition Frontieres, p467

Lea S. M., De Young D. S., 1976, ApJ, 210, 647

Lehnert M., Heckman T., 1996, ApJ, 472, 546

Lu L., Sargent W. L. W., Barlow T. A., Rauch M., 1998, astro-ph/9802189

MacLow M.-M., Ferrara, A., 1998, in *The Magellanic Clouds and Other Dwarf Galaxies*, Eds.: T. Richtler and J.M. Braun, Shaker Verlag, Aachen. (astro-ph/9801237)

MacLow M.-M., McCray R., Norman M. L., 1989, ApJ, 337, 141

Mathews W., 1972, ApJ, 174, 101

Marlowe A. T., Heckman T. M., Wyse R. F. G., Schommer, R., 1995, ApJ, 438, 563

Meurer G. R., Freeman K. C., Dopita M. A., Cacciari C., 1992, AJ, 103, 60

Moore B., Katz N., Lake G., Dressler A., 1996, Nature, 379, 613

Moore B., Lake G., Katz N., 1998, ApJ, 495, 139

Murakami I., Ikeuchi S., 1994, ApJ, 420, 68

Nagasawa M., Nakamura T., Miyama S. M., 1988, PASJ, 40, 691

Navarro J. F., Steinmetz M., 1997, ApJ, 478, 13

Norman C., Spaans M., 1997, ApJ, 480, 145

Norman M. L., Winkler K-H. A., 1986, in *Astrophysical Radiation Hydrodynamics*, Eds: K-H. A. Winkler, M. L. Norman,

Dordrecht, Reidel, p. 187

Nulsen P. E. J., 1982, MNRAS, 198, 1007

Peterson R. C., Caldwell N., 1993, AJ, 105, 1411

Portnoy D., Pistinner S., Shaviv G., 1993, ApJS, 86, 95

Quinn T., Katz N., Efstathiou G., 1996, MNRAS, 278, L49

Raymond J. C., Cox D. P., Smith B. W., 1976, ApJ, 204, 290

Rees M. J., 1986, MNRAS, 218, 25p

Rieke G., Loken L., Rieke M., Tamblyn P. 1993, ApJ, 214, 99

Saito M., 1979, PASJ, 31, 193

Secker J., 1996, ApJ, 469, L81

Secker J., Harris W.E., Plummer J. D., 1997, PASP, 10, 1377

Silk J., Wyse, R.F.G., Shields, G.A., 1987, ApJ, 322, L59

Songaila A., Cowie L.L., 1996, AJ, 112, 335

Spaans M., Norman C., 1997, ApJ, 483, 87

Takeda H., Nulsen P. E. J., Fabian A. C., 1984 MNRAS, 208, 279

Theuns T., Warren S. J., 1997, MNRAS, 284, L11

Thoul A. A., & Weinberg D. H., 1996, ApJ, 465, 608

Thuan T. X., Alimi J.-R., Gott J. R. III, Schneider S. E., 1991, ApJ, 370, 25

Tolstoy E. 1999, astro-ph/9901245

Toyama K., Ikeuchi S., 1980, Progress Theor. Phys. 64, 831

Trentham N., 1998, MNRAS, 294, 193

Tytler D., Fan X.-M., Burles S., Cottrell L., Davis C., Kirkman D., Zuo L., 1995, in *QSO Absorption Lines*, Ed: G. Meylan, Springer-Verlag.

Umemura M., Ikeuchi S., 1984, Prog. Theor. Phys., 72, 47

Vader J. P., 1986, ApJ, 305, 669

Vader J. P., Chaboyer B., 1993, AJ, 108, 1209

Vader J. P., Sandage A., 1991, ApJ, 379, L1

Van den Bergh S., 1994, ApJ, 428, 617

Wang B., 1995, ApJ, 444, L17

White S. D. W., Frenk C. S., 1991, ApJ, 379, 52

Yoshioka S., Ikeuchi S., 1990, ApJ, 360, 352

**Table 1.** IGM Conditions

| Model | C† | $\widetilde{P}_{\rm IGM}$ | $T_{\rm IGM}$ | $n_{\rm ex}$ | $V_{\rm flow}$ | $R_{\rm max}$ |
|---|---|---|---|---|---|---|
| 5P | P | $10^5$ | $10^7$ | $10^{-2}$ | 0. | 1.5 |
| 4P | P | $10^4$ | $10^7$ | $10^{-3}$ | 0. | 3.8 |
| 3P | P | $10^3$ | $10^7$ | $10^{-4}$ | 0. | 8.8 |
| 2P | P | $10^2$ | $10^7$ | $10^{-5}$ | 0. | 18.0 |
| 0P | P | $10^0$ | $10^4$ | $10^{-4}$ | 0. | $> 40$ |
| 5M | M | $10^5$ | $10^7$ | $10^{-2}$ | 0. | 1.5 |
| 4M | M | $10^4$ | $10^7$ | $10^{-3}$ | 0. | 3.6 |
| 3M | M | $10^3$ | $10^7$ | $10^{-4}$ | 0. | 8.6 |
| 2M | M | $10^2$ | $10^7$ | $10^{-5}$ | 0. | 18.0 |
| 0M | M | $10^0$ | $10^4$ | $10^{-4}$ | 0. | $> 40$ |
| -2M | M | $10^{-2}$ | $10^4$ | $10^{-6}$ | 0. | $> 40$ |
| 5PW | P | $10^5$ | $10^7$ | $10^{-2}$ | 1000. | |
| 4PW | P | $10^4$ | $10^7$ | $10^{-3}$ | 1000. | |
| 3PW | P | $10^3$ | $10^7$ | $10^{-4}$ | 1000. | |
| 5MW | M | $10^5$ | $10^7$ | $10^{-2}$ | 1000. | |
| 4MW | M | $10^4$ | $10^7$ | $10^{-3}$ | 1000. | |
| 3MW | M | $10^3$ | $10^7$ | $10^{-4}$ | 1000. | |
| 3MW6 | M | $10^3$ | $10^7$ | $10^{-4}$ | 600. | |
| 2MW4 | M | $10^2$ | $10^7$ | $10^{-5}$ | 400. | |

Units are Kcm$^{-3}$ for $\widetilde{P}_{\rm IGM}$; K for $T_{\rm IGM}$; cm$^{-3}$ for $n_{\rm ex}$; km s$^{-1}$ for $V_{\rm flow}$; and kpc for $R_{\rm max}$.
† Cooling function: P for primordial cooling and M for metal cooling.

( murakami-fig1.gif )

**Figure 1.** Snapshots of isodensity contour and velocity field in r-z plane for model -2M. Density profiles ($g\ cm^{-3}$) for the cross section at r=0kpc (solid line) and 2kpc (dotted line) are also shown. The time measure from the beginning of the simulation is shown at upper right corner and 3.8E7yr means $3.8 \times 10^7$ yr. The contour level is set as $\Delta \log \rho = 0.25$.

( murakami-fig2.gif )

**Figure 2.** The same as Figure 1 but for model 0M.

( murakami-fig3.gif )

**Figure 3.** The same as Figure 1 but for model 3M.

( murakami-fig4.gif )

**Figure 4.** The same as Figure 1 but for model 4M.

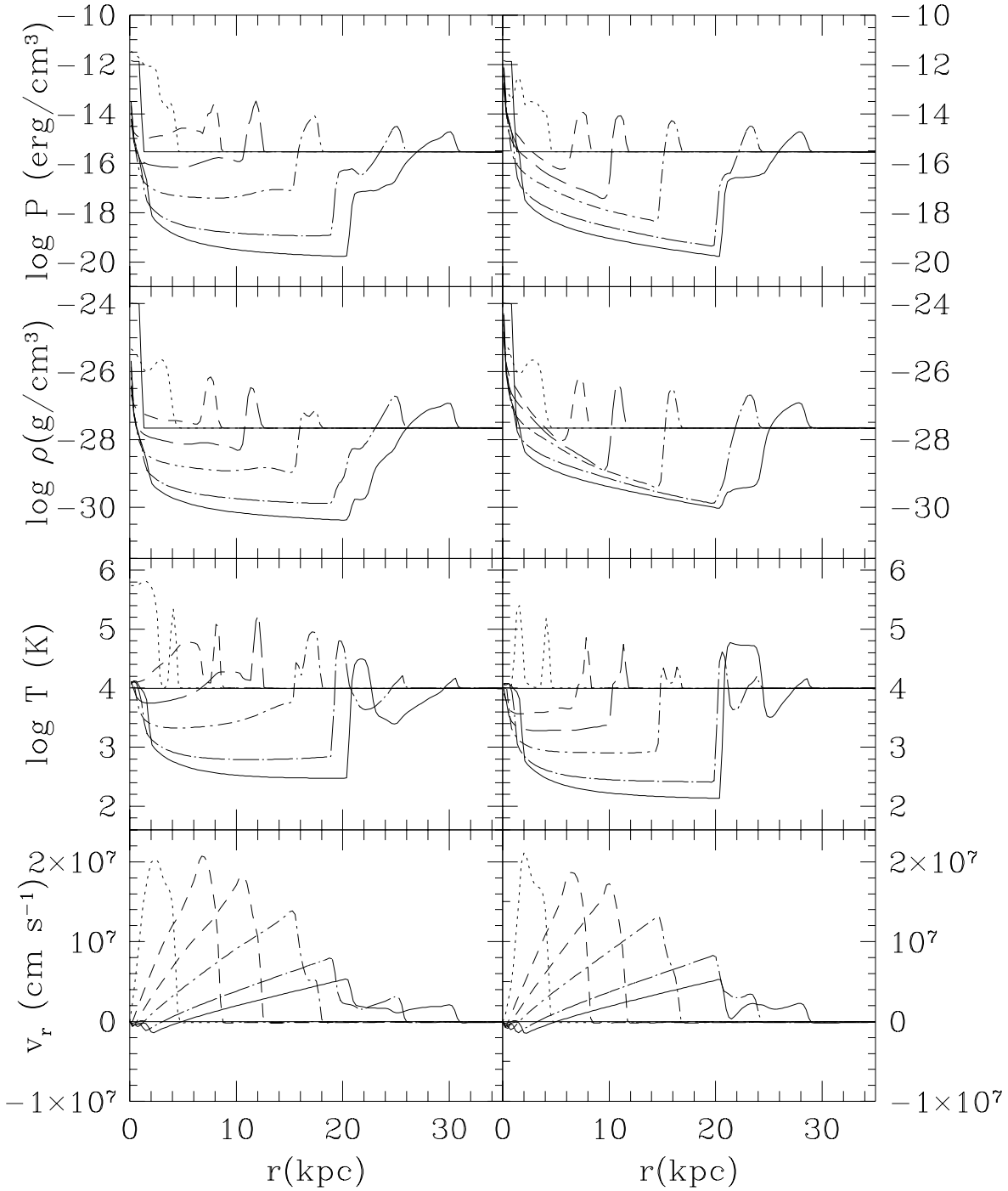


**Figure 5.** Profiles of pressure, density, temperature and velocity (r component) at the cross section at z=0kpc for model 0P (left) and 0M (right). The time for each line is initial state (solid line), $2.4 \times 10^7$ yr (dotted), $4.8 \times 10^7$ yr (dashed), $7.2 \times 10^7$ yr (long dashed), $1.2 \times 10^8$ yr (dot-dashed), $2.4 \times 10^8$ yr (long dash-dotted), and $3.6 \times 10^8$ yr (solid).

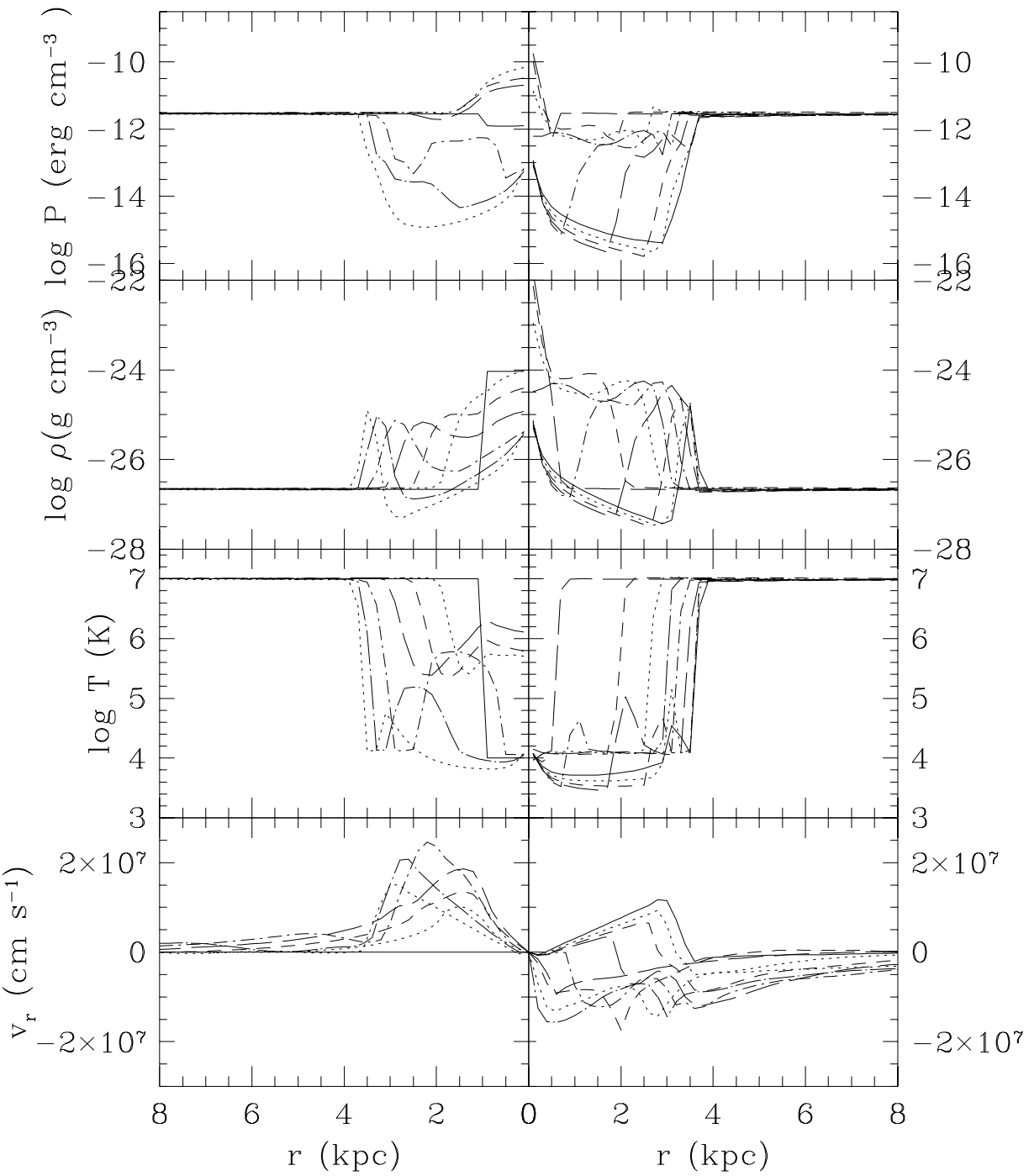


**Figure 6.** Profiles of pressure, density, temperature and velocity (r component) at the cross section at z=0kpc for model 4M expanding phase(left) and collapsing phase (right). The time for each line is initial state (solid line, left panel), $9.5 \times 10^6$ yr (dotted, left), $1.4 \times 10^7$ yr (dashed, left), $1.9 \times 10^7$ yr (long dashed, left), $2.4 \times 10^7$ yr (dot-dashed, left), $2.9 \times 10^7$ yr (long dash-dotted, left), $3.3 \times 10^7$ yr (dotted, left), $3.8 \times 10^7$ yr (solid, right), $4.3 \times 10^6$ yr (dotted, right), $4.7 \times 10^7$ yr (dashed, right), $5.2 \times 10^7$ yr (long dashed, right), $5.7 \times 10^7$ yr (dot-dashed, right), $6.2 \times 10^7$ yr (long dash-dotted, right), $6.6 \times 10^7$ yr (dotted, right), $7.6 \times 10^7$ yr (dashed, right), and $9.5 \times 10^7$ yr (long dashed, right).

© 0000 RAS, MNRAS **000**, 000–000

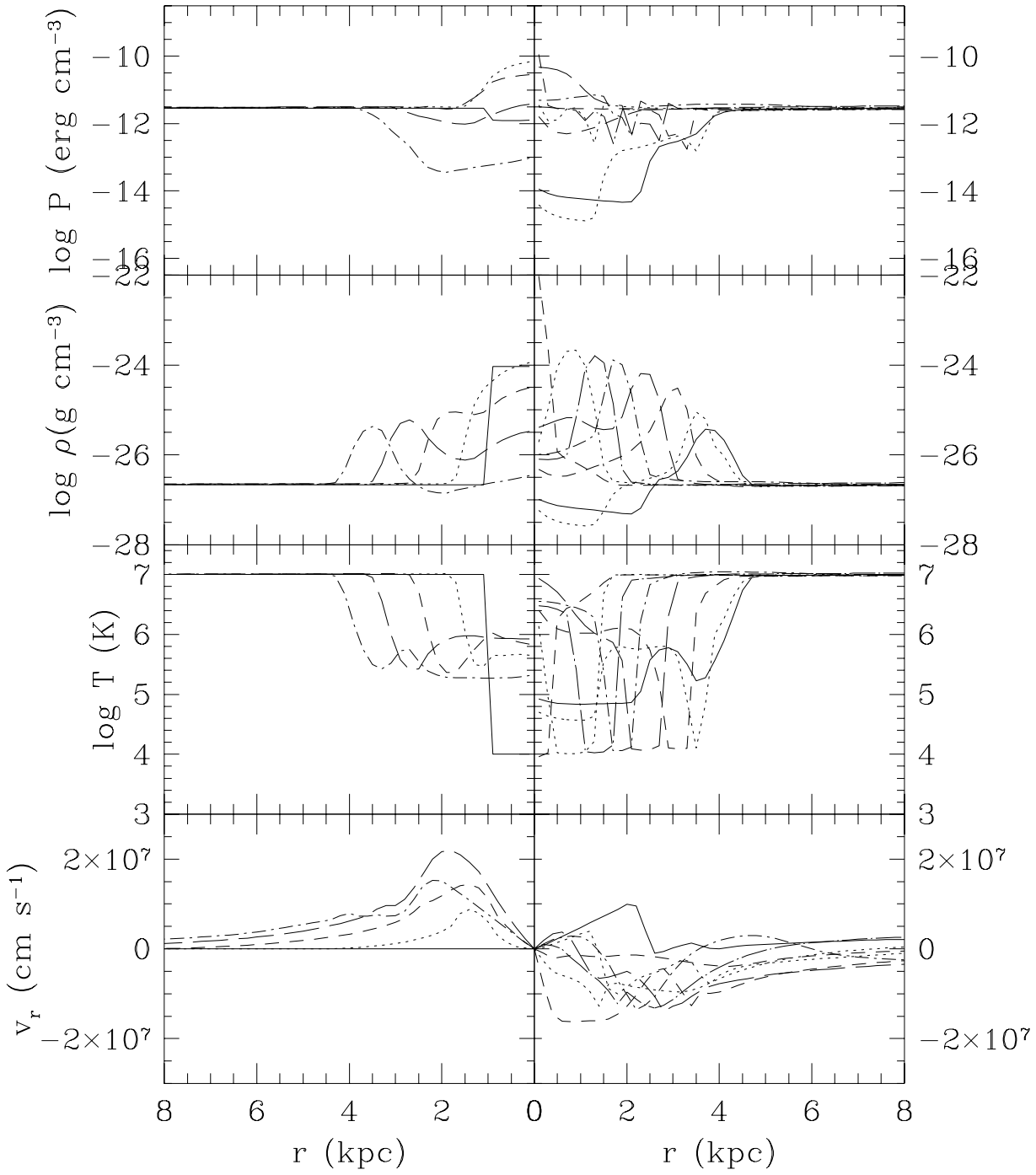


**Figure 7.** Profiles of pressure, density, temperature and velocity (r component) at the cross section at z=0kpc for model 4P expanding phase(left) and collapsing phase (right). The time for each line is initial state (solid line, left panel), $7.6 \times 10^6$ yr (dotted, left), $1.5 \times 10^7$ yr (dashed, left), $2.3 \times 10^7$ yr (long dashed, left), $3.0 \times 10^7$ yr (dot-dashed, left), $3.8 \times 10^7$ yr (solid, right), $4.6 \times 10^6$ yr (dotted, right), $5.3 \times 10^7$ yr (dashed, right), $6.1 \times 10^7$ yr (long dashed, right), $6.8 \times 10^7$ yr (dot-dashed, right), $7.6 \times 10^7$ yr (long dash-dotted, right), $8.3 \times 10^7$ yr (dotted, right), and $1.1 \times 10^8$ yr (dashed, right).

( murakami-fig8.gif )

**Figure 8.** Snap shots of isodensity contour map in r-z plane for model 3M in collapse phase. The contour level is set as $\Delta \log \rho = 0.25$. (a) and (b) are results from calculation with numerical resolution, dr=0.2kpc; and (c) and (d) are results from calculation with dr=0.1kpc. Density maps of finer numerical resolution show thinner collapsing shell and many tentacle-like features due to the instability. 1.04E8yr means $1.04 \times 10^8$ yr.

( murakami-fig9.gif )

**Figure 9.** Snapshots of isodensity contour and velocity field in r-z plane for model 3MW. Density profiles ($g\ cm^{-3}$) for the cross section at r=0kpc (solid line), 2kpc (dotted line), and 5kpc (dashed line) are also shown. The time measure from the beginning of the simulation is shown at upper right corner and 4.3E7yr means $4.3 \times 10^7$ yr. The contour level is set as $\Delta \log \rho = 0.25$.

( murakami-fig10.gif )

**Figure 10.** Snapshots of isodensity contour and velocity field in r-z plane for model 5MW. Density profiles ($g\ cm^{-3}$) for the cross section at r=0kpc (solid line) and 1kpc (dotted line) are also shown. The contour level is set as $\Delta \log \rho = 0.25$.

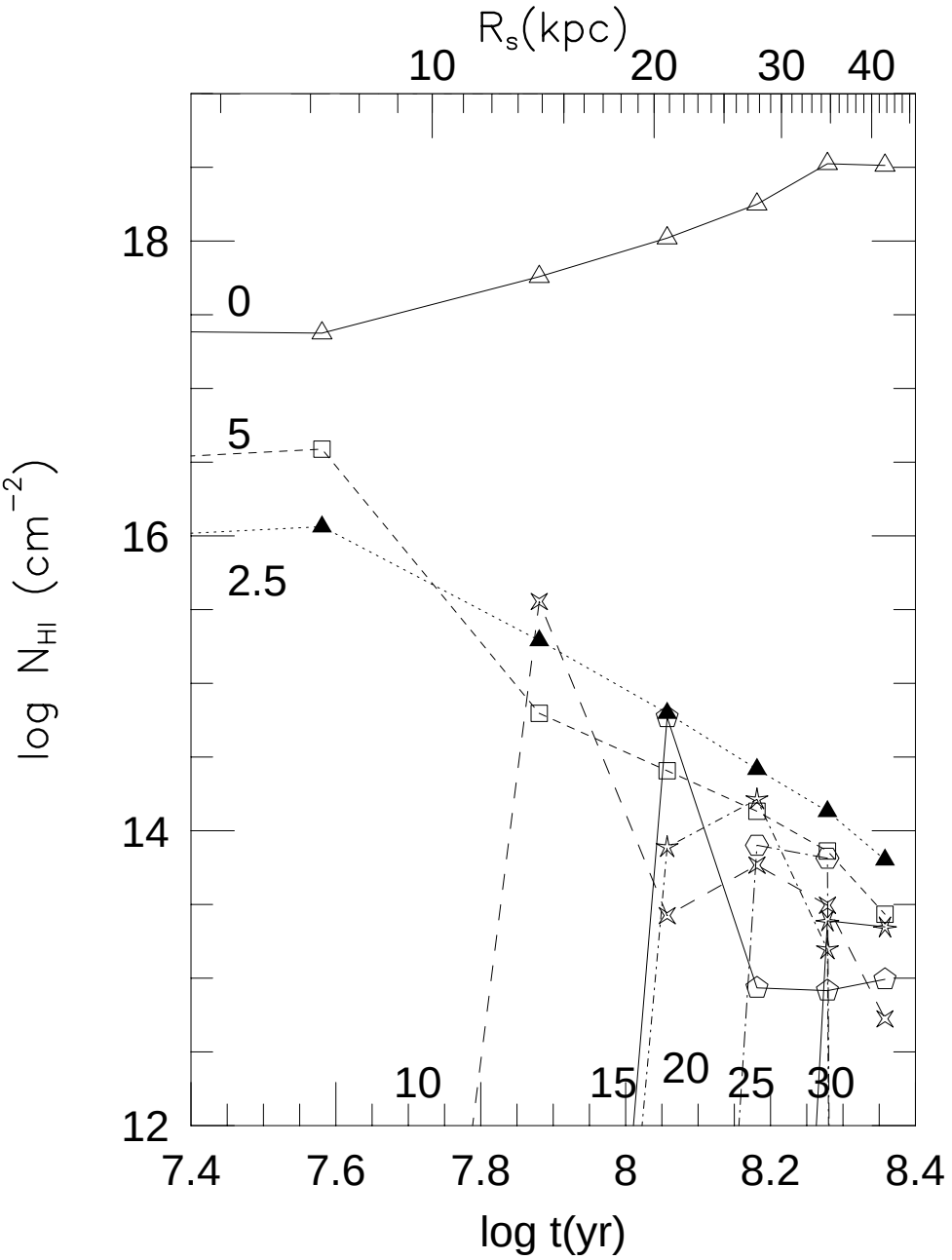


**Figure 11.** Time evolution of HI column densities for fixed sight lines for mode -2M. $J_0 = 1.0 \times 10^{-21}$erg s$^{-1}$cm$^{-2}$Hz$^{-1}$str$^{-1}$ is assumed for the background UV flux. Each line is labeled with the impact parameters. The contribution of the IGM to the column densities is neglected. The radius of the expanding shell is indicated as the upper horizontal axis.

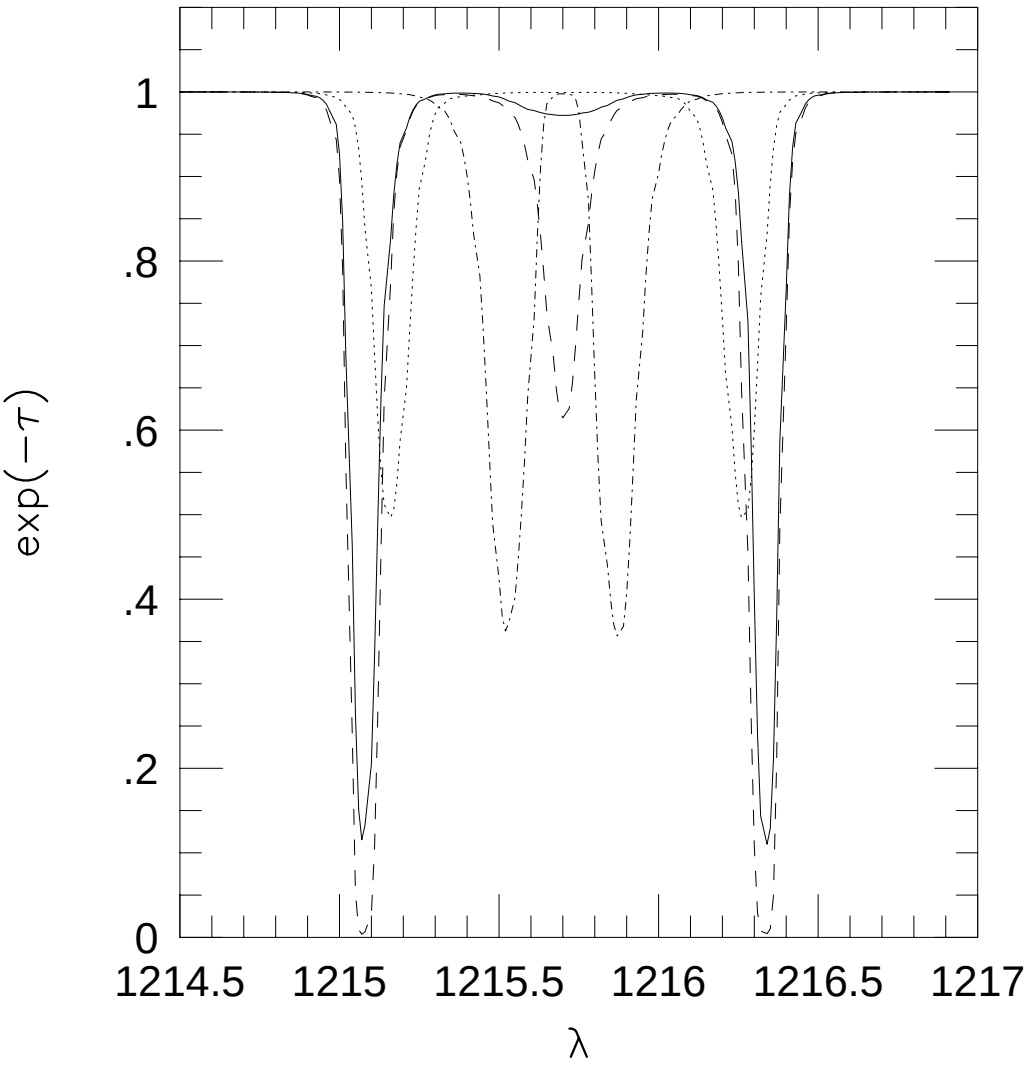


**Figure 12.** Expected absorption profiles for model -2M at t=1.9 $\times 10^8$yr. Impact parameters of sight lines are 5kpc (dashed line), 10kpc (solid line), 20kpc (dotted line), and 30kpc (dot-dashed line). $J_0 = 1.0 \times 10^{-21}$erg s$^{-1}$cm$^{-2}$Hz$^{-1}$str$^{-1}$ is assumed for the background UV flux.

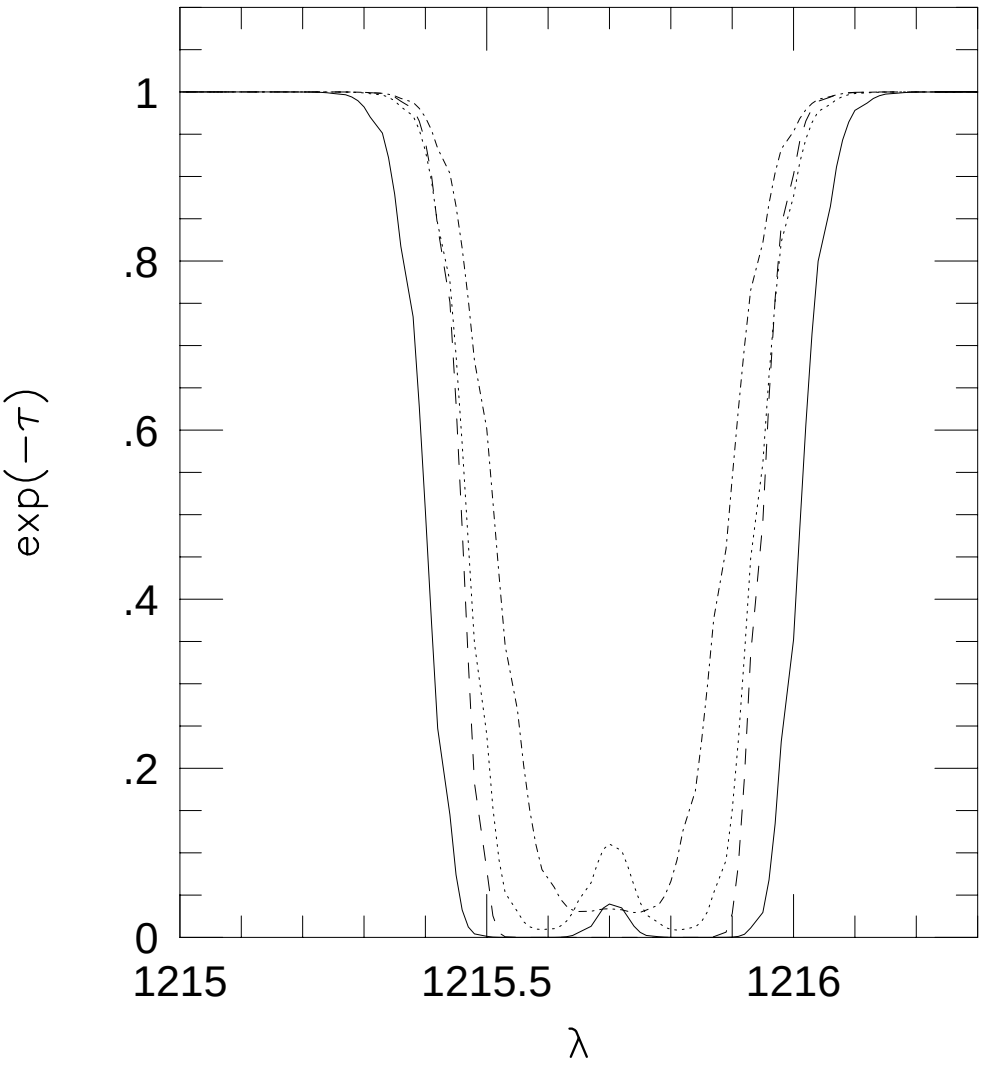


**Figure 13.** Expected absorption profiles for model 0M at t=2.9 $\times 10^8$yr. Impact parameters of sight lines are 10kpc (solid line), 15kpc (dotted line), 20kpc (dot-dashed line), and 25kpc(dashed line). $J_0 = 1.0 \times 10^{-21}$erg s$^{-1}$cm$^{-2}$Hz$^{-1}$sr$^{-1}$ is assumed for the background UV flux.

This figure "murakami-fig1.gif" is available in "gif" format from:
http://arXiv.org/ps/astro-ph/9906084v1

This figure "murakami-fig2.gif" is available in "gif" format from:
http://arXiv.org/ps/astro-ph/9906084v1

This figure "murakami-fig3.gif" is available in "gif" format from:
http://arXiv.org/ps/astro-ph/9906084v1

This figure "murakami-fig4.gif" is available in "gif" format from:
http://arXiv.org/ps/astro-ph/9906084v1

This figure "murakami-fig8.gif" is available in "gif" format from:
http://arXiv.org/ps/astro-ph/9906084v1

This figure "murakami-fig9.gif" is available in "gif" format from:
http://arXiv.org/ps/astro-ph/9906084v1

This figure "murakami-fig10.gif" is available in "gif" format from:
http://arXiv.org/ps/astro-ph/9906084v1